HIGH SPEED SECONDARY GAS INJECTION IN FLUIDIZED BEDS: FLOW PATTERN ANALYSIS BY FAST X-RAY COMPUTED TOMOGRAPHY

Benedikt Köninger[1], Timo Hensler[1], Sebastian Schug[2], Wolfgang Arlt[2], Karl-Ernst Wirth[1]

[1] *Institute of Particle Technology, Friedrich-Alexander Universität Erlangen-Nürnberg, Cauerstraße 4, 91058 Erlangen, Germany*

[2] *Institute of Separation Science & Technology, Friedrich-Alexander Universität Erlangen-Nürnberg, Egerlandstraße 3, 91058 Erlangen, Germany*

*Email: *Karl-Ernst.Wirth@fau.de*

Abstract

This study investigates the secondary gas injection into fluidized and fixed beds with a jet velocity up to 500 ms^{-1}. The flow is examined with a non-invasive measuring technique, a fast rotating X-ray computed tomography (CT). As bed material, glass-bead fractions with narrow particle size distribution in the range between $x_{1,2}$ = 60 and 160 µm were used. By adapting the exposure time as well as filtering the radiation, the picture quality could be decisively increased. Thus, the jet morphology was investigated for different operating conditions. Higher jet velocities showed low time fluctuations with a higher penetration into the bed. Fluidization of the bed material leads to a bending of the jet, but increases the mixing and entrainment around the jet cavity. This area around the jet becomes more pronounced with increasing particle size, but disappears almost completely in the fluidized state. By determining the jet length with the obtained data, a good agreement was found with values from the literature.

INTRODUCTION

Fluidized bed reactors are characterized by homogenous solids mixing, resulting in many applications in the industry. For some processes a fast contact between gas and particles is a decisive point. One possibility of process control is to inject a reaction gas by means of nozzles. The injected gas forms a multiphase jet which can act as a reactor or as an exchange unit (Roach, 1993). This method also prevents undesired wall effects with the reaction gas. One side effect is the appearance of abrasion or breakage between the particles caused by the high energy input. This circumstance can be used to control the particle size in the fluidized bed reactor. One example is the fluid coking process in the production of crude oil (McMillan, 2007). Another application is the fine grinding in fluidized bed opposed jet mills, which work according to the principle of secondary gas injection. In these mills, high-speed gas jets are used to grind even the hardest materials into the submicron range (Berthiaux, 1999). For improving existing processes and developing new applications, an understanding of the hydrodynamics of the jet, the resulting movement of gas and solids, is crucial.

Numerical investigation of the flow is expensive in computational resources and time. A high gas velocity forces the use of small time steps and mesh sizes. A further problem is the modeling of the interaction between the low loaded jet flow and the highly loaded fluidized/fixed bed. In addition, the obtained simulative results must be validated. For this reason, an experimental investigation of secondary gas injection is still the subject of current research.

A first step to characterize a multiphase jet is the determination of the jet length. (Hong, 1997). Two major problems arise in the experimental investigation of the flow. First there is no natural optical access to the jet since a high solids concentration is present at the boundary. This problem can be solved by using a two-dimensional fluidized bed, having a glass plate for optical access. This possibility of flow visualization is applied in many studies, for example in the work of Agarwal (Agarwal, 2011). With that measurement technique, a number of correlations for vertical and horizontal jet lengths have been obtained (Merry, 1971, Hong, 1997). The second problem arises when probes are used to investigate the flow. Due to the high energy of accelerated particles, damage to the probes can occur due to the sandblasting effect. Both, probes and two-dimensional fluidized bed are invasive measurement techniques and therefore disturb the tender jet flow. For this reason, a non-invasive measurement technique is highly desirable and available in different forms: In the work of Hensler et al. the motion of a single particle in a fluidized bed with secondary gas injection was recorded by using positron emission particle tracking (Hensler, 2015). This allows the determination of the solids distribution as well as the residence time in the jet cavity. Unfortunately this technique is limited to relative large particles (>200 µm) and moderate jet velocities, since breakage or

abrasion of the tracked particles prohibits measurements. A non-invasive analysis of fluid-solid flows is also possible using different tomographic techniques. By using electrical capacitance tomography the solids distribution in a fluidized bed can be determined. The advantage is a high time resolution, but the spatial resolution is limited (van Ommen, 2008). Another method is X-ray computed tomography (CT), which allows the time-averaged determination of the solids concentration (Grassler, 2000). In general, X-ray CT´s show a high spatial resolution and a low time resolution. There are some exceptions, like the ultrafast X-ray CT used by Bieberle & Barthel (Bieberle, 2016). With this CT it is possible to achieve a time resolution of 8 kHz with a spatial resolution down to 1 mm. In the work of Franka & Heindel the effect of secondary gas injection on the local time-averaged holdup is investigated by using X-ray CT (Franka, 2009). However, relatively large particles were used on the one hand and low jet velocities on the other hand in previous publications.

Since there is little data for small particles combined with high jet velocities in the literature, this article presents an investigation of the flow pattern in a fluidized bed with secondary gas injection. For this purpose a modern X-ray CT unit is used to access the turbulent flow. The influence of the particle size was investigated from $x_{1,2}$ =60 to 160 µm and the jet velocity was varied from 50 to 500 ms^{-1}. Additionally the influence of the fluidization condition was examined. CT scans obtained with the measurements were used to determine the jet length and were compared with literature data.

X-RAY COMPUTED TOMOGRAPHIE

X-ray computed tomography (CT) is a non-invasive measurement technique and is widely used for medical imaging since the 1970s (Brenner, 2007). Since X-rays have the ability to penetrate matter, it is possible to gain information of the inner structure of objects. For that reason, this technique is highly interesting for analyzing multiphase flows like fluidized beds (Maurer, 2015). In general, the CT consist of a rotating frame, the gantry unit, on which the X-ray source and detector are attached on opposed sides. This working principle is schematically shown in Fig 1. On one side, the X-ray source irradiates the object to be examined by a fan beam (S_1). When the radiation hits matter, it is attenuated depending on the composition of the material. On the opposite side is a line detector, which detects the incoming photons. This results in an intensity distribution (I_1) or a so-called projection. If an object is in the beam path, the intensity is attenuated. Then a further intensity distribution (I_2) is recorded at a new position (S_2) by a rotation of the X-ray source and the detector.

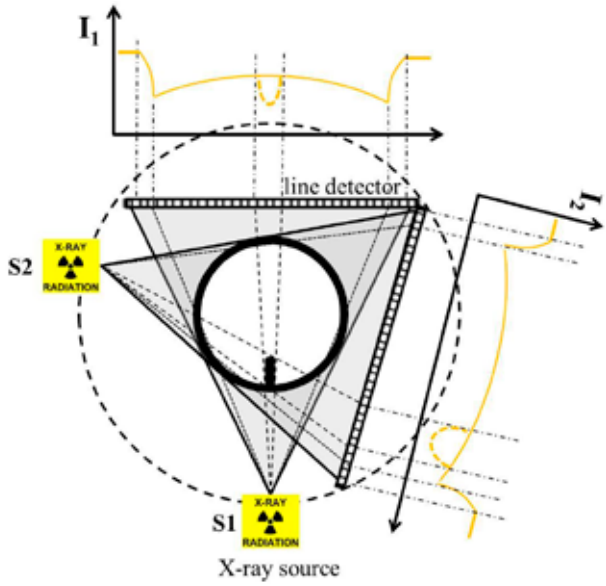

Fig. 1. Schematic working principle of X-ray tomographic measurements

The attenuation, when radiation is passing through a homogeneous object, can be described by using Beer-Lambert law for monochromatic radiation:

$$\frac{I}{I_0} = e^{-\mu L} \tag{1}$$

In Eq. 1, I represents the transmitted and I_0 the incident intensity, while μ is the linear attenuation coefficient of the object and L is the path length of the penetration.

Since X-ray sources produce polychromatic radiation spectra, the attenuation can be described by a modified Beer-Lambert law (Meng, 2009):

$$I = I_0 \int_0^{E_{max}} S(E)\, e^{-\int_0^L \mu(E) dL} dE \tag{2}$$

Eq. 2 takes into account that the incident X-ray spectrum S(E) and the linear attenuation coefficient μ(E) are dependent on the energy E of the penetrating photon. The equations for the attenuation in dispersed systems must be adapted such as shown in Eq. 3 for the case of monochromatic radiation (Hensler, 2016):

$$\frac{I}{I_0} = e^{-\mu L(1-\varepsilon)} \tag{3}$$

In this case, the effectively irradiated length is adapted with the term L(1-ε), whereby the cavities of the bed are also taken into account. By strongly filtering the X-ray radiation, the polychromatic spectra approaches the monochromatic case.

EXPERIMENTAL SETUP & MATERIAL

The experimental studies were performed in a fluidized bed with an inner diameter of 94 mm. By choosing acrylic glass of 3 mm thickness as wall material, the attenuation caused by the pipe is kept at minimum. In the bottom a sintered steel plate distributes the fluidization gas equally. In 75 mm height three horizontal nozzles are arranged in a 120° distance to each other. The identical cylindrical nozzles, made of polyamide, have a 2 mm inner diameter (d_0) and its exit is in a 5 mm distance to the column wall. Before the experiments the column was filled with 1.2 kg of solids, which corresponds to a filling height of about 130 mm. On the top, a settling zone with an inner diameter of 180 mm and a filter keeps the solids inside the column. A schematic representation of the setup, including spatial dimensions as well as the nozzle design can be seen in Fig. 2. The fluidization gas and the secondary gas injection are controlled by separate mass flow controllers. In this work just one single nozzle is operated, which minimizes the problem of solid transport out of the region of interest. The applied jet velocities are defined as the volume flow rate divided by the nozzle cross-section at the exit.

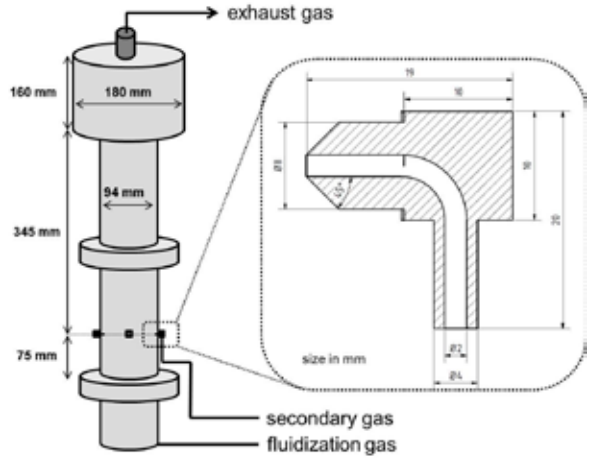

Fig. 2. Schematic representation of the fluidized bed and the used nozzle

The measurements were performed using an X-ray gantry CT developed by Fraunhofer EZRT (Fürth, Germany), described in detail in the works of Schug & Arlt (Schug, 2015, Schug 2016). While the fluidized bed is fixed in the center, the whole gantry unit is constantly rotating (on-the-fly measurement). In one rotation 750 projections are recorded for the calculation of a CT image. Therefore a back-projection reconstruction algorithm (Volex by Fraunhofer) is applied resulting in a gray value image. The setup allows a maximum rotation speed of 1 rpm, having an exposure time of 2 ms per projection. Measurements with these conditions (2 ms exposure time, no filter) lead to images with strong ring artifacts, mainly caused by beam hardening. To reduce this effect, a 1 mm stainless steel filter was installed on the X-ray source. Since the filter is reducing the number of photons arriving the detector, the exposure time must be increased. An exposure time of 10 ms (7.5 s per rotation) delivered a good signal to noise ratio without losing too much time information. Additionally, it is also possible to change the scanning height in a matter of seconds, but in this work the measurement height was fixed to the center of the nozzle. The X-ray source was operated with an acceleration voltage of 140 kV and a current of 2.8 mA. After processing the raw data, a reconstructed 8-bit grayscale image with 1533 x 1533 pixels is received with a spatial resolution of 83 µm. This is in the range of the used particles.

In this work soda-lime glass beads (Sigmund Lindner, Germany) with narrow size distributions (see Fig 3) were used. The solid shows a good flowability and tends not to stick at the wall. For this reason, the bed holdup can be considered constant during the measurements if particle entrainment is negligible. Due to its high hardness, the change of particle size during the experiments can be neglected. The minimum fluidization velocity u_{mf}, determined by pressure drop measurements, increases almost linearly with the Sauter mean diameter $x_{1,2}$ and is included in Fig 3 as well as the calculated single particle settling velocity u_{sv}.

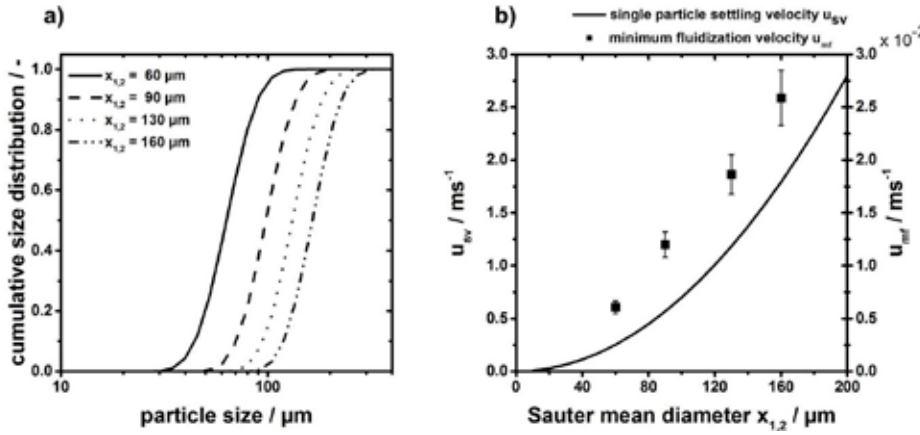

Fig. 3. Particle size distribution of the used glass bead fractions (a) and the associated minimum fluidization velocity as well as the single particle settling velocity (b)

According to Meng et al., the linear attenuation coefficient µ of glass beads stays almost constant when the energy of the X-rays exceeds 100 keV (Meng, 2009). This means that beam hardening occurs below 100 keV. The used steel filter reduces the proportion of low-energy radiation resulting in the described image quality is the result.

RESULTS AND DISCUSSION

Fig. 4 shows an example of a CT scan using glass beads with a Sauter mean diameter of $x_{1,2}$ = 90 µm and a jet velocity u_0 of 100 ms^{-1}. This image is a time average of 5 consecutive images (5 integrations). Regions of high solids concentrations appear in light grey can thus be distinguished clearly from region of low solids concentration, appearing in darker color. The image shows almost no ring artifacts, which is a result of the filtering. In addition, the column wall and the polymer nozzles are distinctly different in color from the solids and the gas. The effluent gas forms a cavity, which stands out sharply from the surrounding solid. Using the gray values from the images, the solids distribution can be visualized in color. Simplifying, a linear fit between gas ((1-ε)=0) and fixed bed ((1-ε)=0.55) was taken here in order to obtain a qualitative distribution of solids. This makes the very thin boundary layer between jet and fixed bed visible (see Fig.4 (b)). Although the images represent a time average of 7.5 seconds, the position of the jets is relatively constant in this case.

By using an 8 bit image, the maximum resolution of the solids concentration is ±0.4 %. For a quantitative determination of the solids distribution, the number of integrations must be increased and a simple calibration method, presented in the work of Hensler et al. (Hensler, 2016), has to be used.

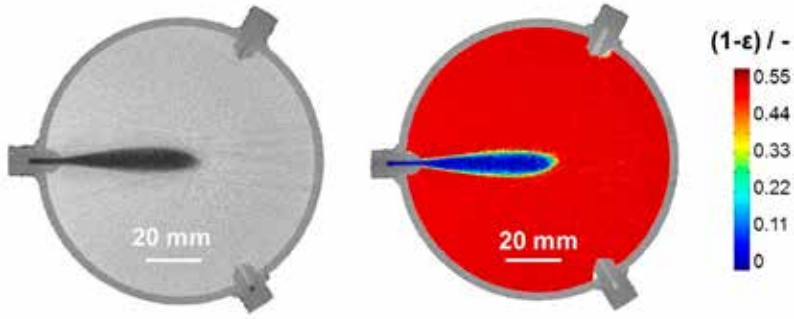

Fig. 4. CT-scan of the jet center for glass beads with $x_{1,2}$ = 90 µm for a jet velocity u_0 of 100 ms^{-1} (a) and the resulting solids distribution (b)

An increase in the gas velocity leads to an expansion of the jet into the fluidized bed. This is shown in Fig 5, together with the influence of the fluidization velocity. In the fixed-bed state, the jet is a compact unit with one dark region, but in the fluidized state there are two areas: The corejet with low solids concentration and a tail at the end with higher loading, visible through the lighter, diffuse area. The fluidization leads to an upward bend of the entire jet. As a result, the turbulent exterior of the jet is located on the geometric jet axis and leads to more fluctuations. This changes the position of the jet from one image to the next resulting in a smearing effect. These time dependent changes are more strongly pronounced applying low gas jet velocities and higher fluidization velocities.

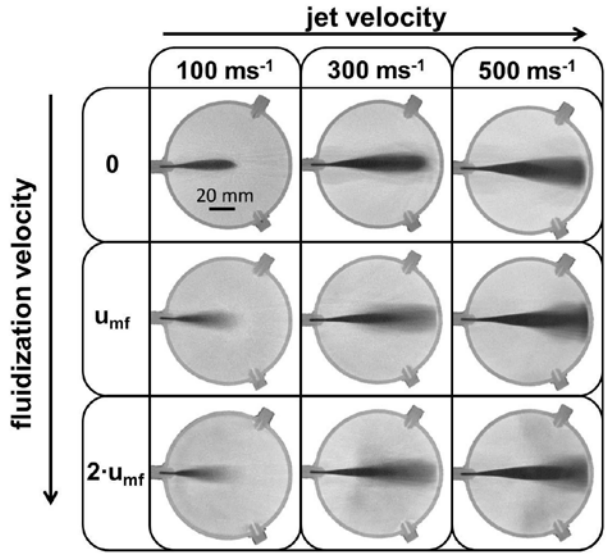

Fig. 5. CT-scan overview of the jet center for glass beads with $x_{1,2}$ = 90 µm

However, when the gas jet velocity is increased above 300 ms^{-1}, the jet contacts the column wall and the whole flow structure at the jet ending is influenced and fluctuations are enhanced. A slightly darker area can be observed around the jet in the fixed bed condition. Since this effect also occurs at the nozzle outlet, where any time fluctuations hardly exist, this is a stationary effect. Here, a lower solids concentration is present, which can be a consequence of gas escaping from the jet and entering the surrounding suspension phase. Another reason may be the entrainment of the particles into the jet. Under fixed bed conditions, particle

mobility is restricted, which limits the transport into the boundary area between jet and fixed bed. For this reason, this phenomenon is less pronounced in the fluidized state.
In addition to fluidization and jet gas velocity, the morphology of the jet is also influenced by the particle size in the bed. For this reason, the particle size was varied between 60 and 160 µm, as shown in Fig.6 for a jet gas velocity of 300 ms^{-1}. By increasing the particle size, the jet formed becomes narrower. For larger particles, the dark area around the jet is increased. This region occurs, in particular, in the vicinity of the nozzle in which, according to Merry (Merry, 1971), the particles are mainly entrained. This effect disappears, with exception of the smallest particles ($x_{1,2}$ = 60 µm), when the bed is fluidized. In general, the morphology is influenced by superimposed and opposing effects. On the one hand, small particles are more likely to be entrained into the jet, which leads to a higher momentum transfer. On the other hand, the higher mobility leads to a lower friction on the boundary surface than on larger particles. Thus, especially in the fluidized state, no exact trend can be determined, since here additionally the effect of jet bending is added. However, at the end of the jet, a larger diffuse region around the boundary layer is observed with increasing particle size. In this area a strong mixing must occur, as accelerated particles from the jet penetrate into the bed. In addition to the enhanced mixing, this momentum exchange can also lead to the comminution of the particles.

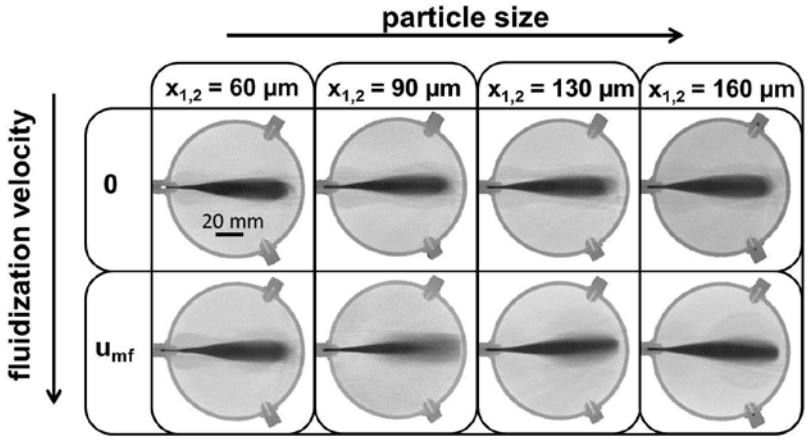

Fig. 6. CT-scan overview for different particle sizes with 300 ms^{-1} jet velocity

The time-averaged X-ray CT images can be used to determine the jet length for different operating parameters. For this purpose, the gray values on the central jet axis are read and evaluated. The transition point between the gray values of the dark gas phase and the light solids phase is defined as the jet end. In most cases, this transition area is very sharp, but can be broadened by the jet bending effect. Therefore, the jet lengths obtained are slightly shorter in the fluidized state as shown in Fig.7 (a). A further increase in the fluidization velocity has no visible effect on the penetration. The presence of bubbles, occurring at $2 \cdot u_{mf}$, does not affect the spread of the jet significantly. The occurrence of bubbles affects the bending of the jet slightly since the momentum of the jet is significantly higher than that of the bubbles. Fig.7 (a) illustrates that the jet length increases linearly with the jet speed in the considered range, with the jet already touching the wall at 500 ms^{-1}.

Two correlations for horizontal jet lengths were used to validate the experimental data gained by CT measurements. The first is the correlation of Merry and is described in Eq.4 (Merry, 1971) and the second one is from Hong and is shown in Eq.5 (Hong, 1997).

$$\frac{L}{d_0} + 4.5 = 5.25 \left(\frac{\rho_f u_0^2}{(1-\varepsilon)\rho_s g d_p} \right)^{0.4} \left(\frac{\rho_f}{\rho_s} \right)^{0.2} \left(\frac{d_p}{d_0} \right)^{0.2} \tag{4}$$

$$\frac{L}{d_0} + 3.8 = 1.89x10^6 \left(\frac{\rho_f u_0^2}{(1-\varepsilon)\rho_s g d_p} \right)^{0.327} \left(\frac{\rho_f}{\rho_s} \right)^{1.974} \left(\frac{d_p}{d_0} \right)^{-0.040} \tag{5}$$

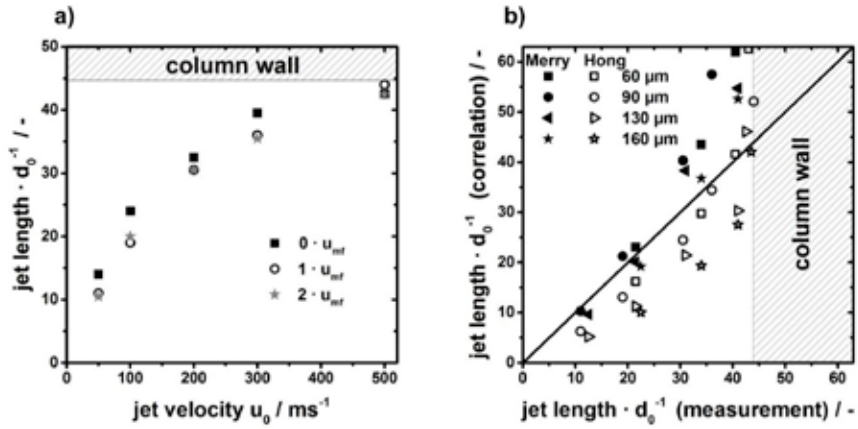

Fig. 7. Determined jet lengths for $x_{1,2}$ = 90 µm (a) and a comparison between the data and the correlations from Merry and Hong (b)

In Fig.7 (b), the dimensionless values obtained from the measurements are plotted against the corresponding calculated dimensionless jet lengths. All points on the solid line represent a perfect match with the respective correlation. In this figure, the data points are plotted for different particle sizes and jet velocities applying minimum fluidization (u_{mf}). In the range of low jet gas velocities ($u_0 \leq 300$ ms^{-1}), the obtained values fit very well to the correlation of Merry. However, there is no clear trend regarding the particle sizes: The jet length is greatest at almost all jet velocities at $x_{1,2}$ = 60 and $x_{1,2}$ = 160 µm. The deviation at higher velocities is mainly due to the interaction of the jet with the wall. On the other hand, with the correlation of Hong, the jet lengths are underestimated. Since Hong uses much larger particles (>1 mm) in his work, this correlation does not match the measurements presented here. It should be noted that in both correlations the determined jet length was defined as the maximum penetration depth of the gas into the bed. Since only the center of the nozzle has been measured here, the maximum jet length can also be larger. A further important point for the deviation is the disturbance of the flow which is not present here. Especially for high gas velocities, the friction at the glass wall cannot be neglected but is included in the correlations.

CONCLUSION

An X-ray computed tomography system was used to investigate the flow structure of a high speed secondary gas injection into a fluidized and fixed bed. The system allows a detailed insight to the jet morphology without disturbing the flow. By using a steel filter and adjusting the exposure time, the occurrence of ring artifacts was almost eliminated. Despite the fast imaging (7.5 s per image), it is possible to clearly distinguish between the jet phase and the fluidized/fixed bed on the basis of the gray values. This also makes it possible to visualize the thin interface between the two phases by means of a simplified solids distribution. It has been shown that the fluidization velocity has a significant influence on the morphology of the jet. An increase in this leads to an upward bending of the jet, resulting in an increased fluctuation and a shorter jet length. The spread of the jet into the bed material can be observed with increased injection speed up to 500 ms^{-1}. An increase in the injection speeds leads to a reduction in the time-dependent fluctuations, which can be seen in a constant position of the jet. Around the jet an area with reduced solids concentration could be observed. Since this occurs mainly in the fixed bed, this is a consequence of the entrainment. In the fluidized bed, the improved flowability allows enough solids to be transported into the region around the jet. In this work the initial particle size of the bed material was also varied ($x_{1,2}$ = 60, 90, 130, 160 µm). When using coarser material, the jet contracts more closely. In addition, the solids-poor area around the jet becomes larger when the gas is injected in a fixed bed. Furthermore, the CT data was used to determine the jet lengths for different operating conditions and bed materials. A good agreement with literature values could be obtained here, even if finer material was used at higher injection velocities. This demonstrates the strength of this non-invasive measurement technique and is to be used in the future to study the exact solids distribution in the area of high speed injection into fluidized and fixed beds.

NOTATION

d_0	nozzle exit diamater, m	d_p	particle diameter, m
E	energy, J	g	gravity constant, ms^{-2}
I	transmitted radiation intensity, -	I_0	incident radiation intensity, -
L	length, m	S	energy spectrum, eV^{-1}
u_0	jet velocity, ms^{-1}	u_{mf}	minimum fluidization velocity, ms^{-1}
u_{sv}	single particle settling velocity, ms^{-1}	$x_{1,2}$	Sauter mean diameter, m
(1-ε)	solids volume fraction, -	μ	attenuation coefficient, m^{-1}
ρ_f	fluid density, kgm^{-3}	ρ_s	solid density, kgm^{-3}

ACKNOWLEDGEMENT

The authors gratefully acknowledge the support by the German Research Foundation DFG within project SPP 1679 through grant number WI 972/23-2. The authors are also thankful to Changwoo Kim, Thomas Linder and Thilo Kögl who supported the experiments.

REFERENCES

Agarwal, G., Lattimer, B., Ekkad S., Vandsburger, U. 2011. Influence of multiple gas inlet jets on fluidized bed hydrodynamics using Particle Image Velocimetry and Digital Image Analysis, Powder Technology. 214, 122-134.

Berthiaux, H., Dodds, J. 1999. Modelling fine grinding in a fluidized bed opposed jet mill: Part I: Batch grinding kinetics. Powder Technology 106, 78-87.

Bieberle, M., Barthel, F. 2016. Combined phase distribution and particle velocity measurement in spout fluidized beds by ultrafast X-ray computed tomography. Chemical Engineering Journal. 285, 218-227.

Brenner, D. J., Hall, E. J. 2007. Computed tomography-An Increasing source of radiation exposure. The New England Journal of Medicine. 357.22, 2277-2284.

Franka N.,. Heindel, T. J. 2009. Local time-averaged gas holdup in a fluidized bed with side air injection using X-ray computed tomography, Powder Technology 193, 69-78.

Grassler, T., Wirth, K.E. 2000. X-ray computer tomography - potential and limitation for the measurement of local solids distribution in circulating fluidized beds, Chemical Engineering Journal 77, 65–72.

Hensler, T., Tupy, M., Strer, T., Pöschel, T., Wirth, K.-E. 2015. Positron emission particle tracking in fluidized beds with secondary gas injection. Powder Technology 279, 113-122.

Hensler, T., Firsching, M., Bonilla, J.S.G., Wörlein, T., Uhlmann N., Wirth, K.-E. 2016 Non-invasive investigation of the cross-sectional solids distribution in CFB risers by X-ray computed tomography, Powder Technology 297, 247-258.

Hong, R. Li, H., Ding J., Li, H. 2005. A Correlation equation for calculating inclined jet penetration length in gas-solid fluidized bed, China Particuology 5, 279-285.

Maurer, S., Wagner, E.C., van Ommen, J.R. , Schildhauer, T.J., Teske, S.L., Biollaz, S.M.A., Wokaun, A., Mudde, R.F. 2015. Influence of vertical internals on a bubbling fluidized bed characterized by X-ray tomography, International Journal of Multiphase Flow 75, 237–249.

McMillan, J., Briens, C., Berruti, F., Chan, E. 2007. High velocity attrition nozzles in fluidized beds. Powder Technology 175, 133–141.

Meng, F., Zhanga, N., Wanga, W. 2009. Virtual experimentation of beam hardening effect in X-ray CT measurement of multiphase flow, Powder Technology 194, 153–157.

Merry, J. 1971. Penetration of a horizontal gas jet into a fluidised bed. Transactions of the Institution of Chemical Engineers and the Chemical Engineer 49, 189-196.

Van Ommen, J.R., Mudde, R.F. 2008. Measuring the gas-solids distribution in fluidized beds - A review. International Journal of Chemical Reactor Engineering 6, 1–29.

Roach, P.E. 1993. The penetration of jets into fluidized beds. Fluid Dynamics Research 11, 197-216.

Schug, S., Arlt, W. 2015. In-situ-Stoffübergangsmessungen mit Computertomographie: Auswahl des Testsystems, Chemie Ingenieur Technik 87, 656-659.

Schug, S., Arlt, W. 2016. Imaging of fluid dynamics in a structured packing using X-ray computed tomography, Chemical Engineering & Technology 39, 1561-1569.